ISSN 1075-7015, Geology of Ore Deposits, 2023, Vol. 65, No. 1, pp. 44–55. © The Author(s), 2023. This article is an open access publication, corrected publication 2023.
Russian Text © The Author(s), 2023, published in Geologiya Rudnykh Mestorozhdenii, 2023, Vol. 65, No. 1, pp. 46–57.

Features of the Interaction of Scheelite with HCl Solutions at 400 and 500°C, 100 MPa, and Various $f(O_2)$ (According to Experimental and Calculated Data)

A. F. Redkin[a], * and N. P. Kotova[a], **

[a] *Korzhinskii Institute of Experimental Mineralogy Russian Academy of Sciences, Chernogolovka, Moscow oblast, 142432 Russia*

**e-mail: redkin@iem.ac.ru*

***e-mail: kotova@iem.ac.ru*

Received May 11, 2022; revised October 3, 2022; accepted October 10, 2022

Abstract—Experimental studies were carried out on the solubility of scheelite in HCl solutions in the concentration range from 0.01 to 0.316 mol/kg H_2O at 400 and 500°C, a pressure of 100 MPa and the fugacity of oxygen (hydrogen) specified by the buffers Cu_2O–CuO, Fe_3O_4–Fe_2O_3, Ni–NiO, and Co–CoO. It was found that scheelite in HCl solutions at the specified parameters dissolves incongruently. In solutions containing from 0.01 to 0.0316 *m* HCl, minor amounts of WO_3 and/or WO_{3-x} tungsten oxides are found in the run products, along with scheelite. In solutions containing from 0.1 to 0.316 *m* HCl, the formation of calcium tungsten bronzes Ca_xWO_3 is observed, the average composition of which corresponds to the formula $Ca_{0.07}WO_3$. Based on the analysis of the experimental data obtained, the free energies of the formation of tungsten oxides WO_3, $WO_{2.9}$, scheelite, and calcium tungsten bronze were calculated. Using mutually agreed thermodynamic data, the solubility of Sch in solutions of HCl and (Na, K)Cl with the participation of aluminosilicates is calculated. It is shown that the scheelite has a wide area of congruent solubility in saline systems.

Keywords: tungsten, calcium, scheelite, tungsten (VI) oxide, calcium tungsten bronze, solubility, chloride solutions, thermodynamic calculations

DOI: 10.1134/S1075701523010063

INTRODUCTION

Scheelite $CaWO_4$ is a very important ore mineral, which includes the element tungsten, which is capable of changing its valency during the transition from the solid phase to the solution. Despite the large number of works that have been devoted to the study of the solubility of this mineral (Khodakovskiy and Mishin, 1971; Forster, 1977; Wood and Samson 2000), the question of the effect of redox conditions on the solubility of scheelite and the valence state of tungsten under hydrothermal conditions has never been considered before. The experimental data available in the literature on the solubility of scheelite in water at low temperatures are not very accurate, which is explained by the low quality of the starting material and its state of aggregation. In studies carried out at high temperatures and pressures (Rafalsky et al., 1984), there is also a low convergence of results on the solubility of scheelite in water and aqueous solutions of KCl. In a sufficiently acidic solution in equilibrium with scheelite, WO_3 was formed, which led to a significant excess of calcium concentration over tungsten (Rafalsky et al., 1984). It was found in (Hu et al., 2011) that, in synthetic nanocrystalline scheelite, the ratio of Ca^{2+} to W^{6+} was 1.2 : 1, which, according to the authors of this publication, could also lead to a change in the ratio of metal ions in solution when this solid phase was dissolved. In connection with the above, the study of the solubility of scheelite in various solutions is of interest for constructing models for the formation of hydrothermal ore-bearing solutions.

EXPERIMENTAL

This paper presents the results of an experimental study of the effect of oxygen fugacity $f(O_2)$ and acidity (*m* HCl) on the solubility of scheelite ($CaWO_4$) at 500 and 400°C and 100 MPa. The starting material was scheelite (Sch) obtained by recrystallization of the chemical reagent $CaWO_4$ (purity grade) in 0.1 *m* HCl at 500°C, 100 MPa, for 20 days and followed by drying at 100°C (Fig. 1). The experiments were carried out in platinum ampoules (7 × 0.2 × 50 mm) sealed by electric arc welding. In experiments at 400°C and 100 MPa, 40 mg of scheelite and 0.8 mL of HCl solution were introduced into a Pt ampoule, while 40 mg of scheelite and 0.65 mL of HCl solution were produced in exper-

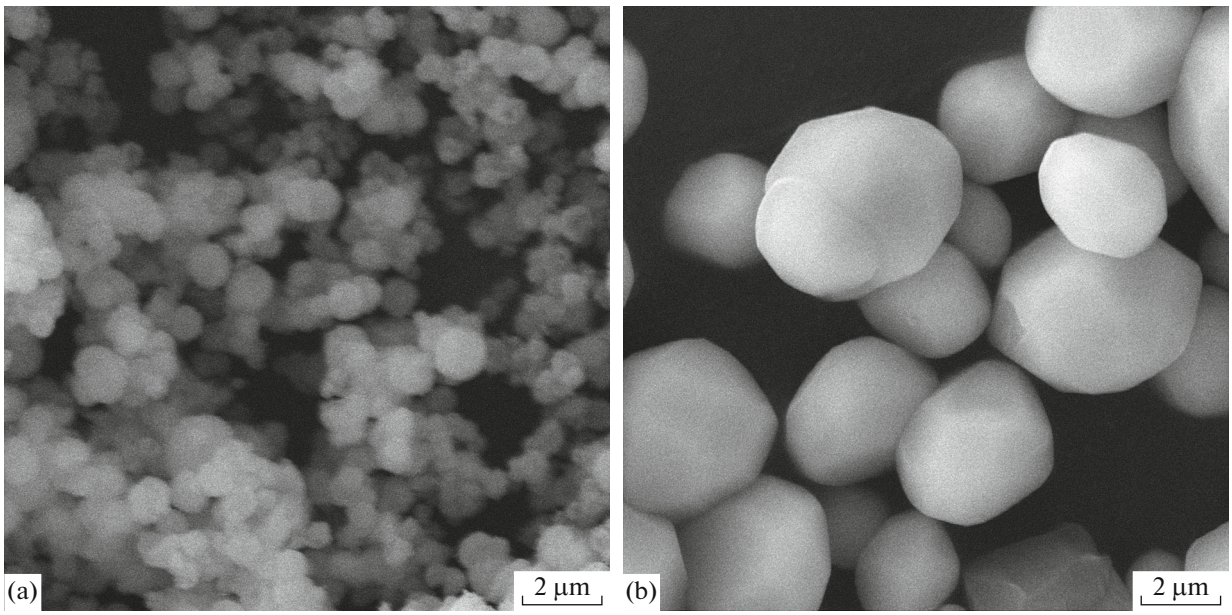

Fig. 1. (a) Initial $CaWO_4$ chemical reagent and (b) the same after recrystallization in 0.1 *m* HCl at 500°C and100 MPa in an experiment lasting 20 days.

iments at 500°C and 100 MPa. To control possible weight loss during the experiments, all ampoules before and after the experiments were weighed on an electronic balance with an accuracy of ±0.01 mg.

The experiments were carried out on a high-pressure hydrothermal installation in reactors with an inner diameter of 30 mm made of NCF80A alloy. Heating was carried out using two-section stoves with a wide (10 cm) gradientless (±3°C) zone. The temperature was measured with armored chromel–alumel thermocouples located inside the reactor at the level of the sample in the ampoule, with an accuracy of ±2°C. The pressure in the system was set using a hydraulic pump with a multiplier using an ultra-high-pressure manometer of SV-2500 type with an accuracy of ±2 MPa.

Four platinum ampoules with the test substance and 0.01, 0.0316, 0.1, and 0.316 molal solutions of HCl were simultaneously loaded into the reactor. The oxygen fugacity in the reactors was set with Co/CoO, Ni/NiO, Fe_3O_4/Fe_2O_3, and Cu_2O/CuO buffer pairs. A cylindrical leaky Ni container with a buffer mixture was placed into the reactor under Pt ampoules. The duration of the experiments was 14 days. After the experiments, the reactors were cooled with a water–air-drop mixture to room temperature for 3–5 min.

The experimental products were transferred from the ampoules to graduated conical polypropylene test tubes, washing the contents of the ampoules three times with distilled water. The total volume was brought to 4.5 mL, and the solution was separated from the solid phases by centrifugation at 6000 rpm. A clean dilute solution was taken for analysis. Dilution control was carried out on an analytical balance. The calcium content in these solutions was determined by the ICP-AES and AAS methods, and the tungsten content was determined by ICP-MS.

The solid products of the experiments dried at 100°C were examined by powder X-ray diffraction and VEGA-TESCAN and Cam Scan MV2300 scanning electron microscopes.

RESEARCH RESULTS

Solution

The liquid phase after the experiments was a colorless solution containing no colloidal suspension. The results of ICP and AAS analyses of solutions after the experiments are presented in Table 1. According to the obtained data, the hydrochloric-acid solution, which was in equilibrium with scheelite, was enriched in calcium and contained relatively low concentrations of tungsten.

Analyses for the determination of calcium in solutions after experiments using the ICP-AES and AAS methods showed similar results (Table 1). According to the obtained data, the calcium concentration in quenched solutions does not depend on the redox conditions ($f(O_2)$). However, it increases with an increase in the concentration of HCl in the initial solution, and the slope angle is $\log m\ Ca_{aq}/m\ HCl_{init}$ close to 1.0 ± 0.1 at 400 and 500°C (Table 2). The calcium content in initial solutions of 0.01, 0.0316, 0.1, and 0.316 *m* HCl was insignificant and amounted to 3.0, 2.2, 1.9, and 16×10^{-5} mol/kg H_2O, respectively.

The concentration of tungsten in the solutions after the experiments, on the contrary, did not depend

Table 1. Results of the analysis of hardened solutions for tungsten (ICP-MS) and calcium (ICP-AES and AAS). The total pressure is 100 MPa. The duration of the experiments is 14 days

				Concentration, mol/kg H_2O			
No.	T, °C	Buffer	$\log f O_2$, Pa	HCl_{ref}	Ca_{aq} ICP-AES	Ca_{aq} AAS	W_{aq} ICP-MS
1	400	Co–CoO	–23.768	0.01	3.628E-03	2.822E-03	1.026E-04
2	400	Co–CoO		0.0316	1.062E-02	9.119E-03	1.022E-04
3	400	Co–CoO		0.1	4.480E-02	3.558E-02	1.018E-04
4	400	Co–CoO		0.316	1.331E-01	1.026E-01	2.443E-05
8	400	Ni–NiO	–22.423	0.01	3.454E-03	7.243E-03	5.577E-05
7	400	Ni–NiO		0.0316	1.157E-02	1.027E-02	9.989E-05
6	400	Ni–NiO		0.1	5.313E-02	4.993E-02	7.621E-05
5	400	Ni–NiO		0.316	1.275E-01	1.081E-01	1.999E-05
9	400	Fe_3O_4–Fe_2O_3	–18.600	0.01	4.052E-03	3.623E-03	2.223E-04
10	400	Fe_3O_4–Fe_2O_3		0.0316	1.049E-02	1.057E-02	1.580E-04
11	400	Fe_3O_4–Fe_2O_3		0.1	3.729E-02	3.816E-02	8.746E-05
12	400	Fe_3O_4–Fe_2O_3		0.316	1.316E-01	1.562E-01	2.925E-05
25	400	Cu_2O–CuO	–6.401	0.01	1.667E-03	3.197E-03	4.988E-04
26	400	Cu_2O–CuO		0.0316	8.636E-03	9.930E-03	2.983E-04
27	400	Cu_2O–CuO		0.1	3.921E-02	3.661E-02	3.981E-04
28	400	Cu_2O–CuO		0.316	1.409E-01	1.255E-01	1.539E-04
13	500	Ni–NiO	–17.706	0.01	3.644E-03	3.341E-03	7.036E-04
14	500	Ni–NiO		0.0316	8.505E-03	9.146E-03	1.332E-03
15	500	Ni–NiO		0.1	2.599E-02	3.034E-02	1.096E-03
16	500	Ni–NiO		0.316	7.740E-02	8.690E-02	1.944E-03
17	500	Co–CoO	–19.089	0.01	3.883E-03	3.102E-03	1.231E-03
18	500	Co–CoO		0.0316	3.804E-03	1.032E-02	8.731E-04
19	500	Co–CoO		0.1	9.913E-03		8.941E-04
20	500	Co–CoO		0.316	1.008E-01	1.033E-01	1.927E-04
21	500	Cu_2O–CuO	–3.567	0.01	3.584E-03	2.754E-03	7.688E-04
22	500	Cu_2O–CuO		0.0316	8.650E-03	8.892E-03	1.062E-03
23	500	Cu_2O–CuO		0.1	3.005E-02	3.583E-02	6.820E-04
24	500	Cu_2O–CuO		0.316	1.118E-01	9.571E-02	2.499E-04

much on m HCl_{init}, but increased when the temperature changed from 400 to 500°C on average by one order of magnitude (by ten times). The effect of redox conditions ($f(O_2)$ on m W_{aq} was determined, but it was ambiguous.

Solid Products of Experiments

The scheelite used in the experiments, which was initially white, changed during the experiment. If in experiments containing 0.01 m HCl, the white color was preserved or a pale yellowish color appeared, then with an increase in the concentration of HCl, the color change was observed from light blue in 0.0316 m HCl to dark blue, in 0.316 m HCl. The intensity of the dark color increased with decreasing $f(O_2)$ from Cu_2O–CuO to Co–CoO buffer. In 0.1 m HCl solutions, in the run products at 500°C, significant recrystallization of scheelite into large individual crystals larger than 100 μm took place. Newly formed black crystals were also present here that had the shape of a polyhedron, similar to that of scheelite crystals. The number of black crystals in experiments with 0.316 m HCl (at 500°C, Ni–NiO and Co–CoO buffers) far exceeded the number of transparent scheelite crystals.

Table 2. Linear dependence coefficients of calcium concentration on hydrochloric acid concentration in equilibrium with scheelite: $\log m\ Ca_{aq} = a + b \log m\ HCl_{init}$

	400°C, 100 MPa		500°C, 100 MPa	
O_2 buffer	*a*	*b*	*a*	*b*
Co–CoO	–0.384 ± 0.058	1.059 ± 0.042	–0.503 ± 0.040	0.981 ± 0.027
Ni–NiO	–0.347 ± 0.080	1.049 ± 0.064	–0.633 ± 0.033	0.923 ± 0.024
Fe_3O_4–Fe_2O_3	–0.347 ± 0.043	1.055 ± 0.031	–	–
Cu_2O–CuO	–0.268 ± 0.076	1.179 ± 0.055	–0.476 ± 0.046	1.025 ± 0.034
Mean value	–0.332 ± 0.035	1.091 ± 0.026	–0.544 ± 0.027	0.974 ± 0.019

Table 3. Calcium content (average, mol) in nonstoichiometric calcium tungstate (calcium–tungsten bronzes) Ca_xWO_3 formed in experiments on the dissolution of scheelite in HCl solutions at 500°C and 100 MPa under various redox conditions

Exp. no.	15	16	19	20	23	24
$\log fO_2$	Ni–NiO	Ni–NiO	Co–CoO	Co–CoO	CuO–Cu_2O	CuO–Cu_2O
m HCl	0.1	0.316	0.1	0.316	0.1	0.316
Sample	11	8	14	12	11	15
Ca	0.075 ± 0.010	0.078 ± 0.007	0.064 ± 0.016	0.072 ± 0.010	0.124 ± 0.019	0.059 ± 0.026

When studying the solid products of experiments on a scanning electron microscope, it was found that, in solutions containing 0.01 *m* HCl, along with scheelite, there are acicular crystals of WO_3, the number of which is very small. In 0.0316 *m* HCl solution, instead of thin needles, columns and rectangular or rhombohedral twin intergrowths of crystals of dark blue color were formed (the color was observed in an optical microscope), which also contained only W and O (WO_{3-x}). Black crystals that formed in solutions containing 0.1 and 0.316 *m* HCl showed a zonal structure during grinding and polishing: inside, they are composed of scheelite, and outside they are covered with a shell of calcium–tungsten bronzes (CTBs) to a depth of 40 μm (Fig. 2). The compositions of the CTB phases are presented in Table 3. CTBs are fine fibrous textures and are the end product of Sch substitution in an acidic environment. The total amount of CaO and WO_3 oxides in tungsten bronzes is lower than in scheelite. This indicates the presence of water in the CTB structure. The removal of calcium from Sch was carried out through channels in the CTB structure, as well as through the intergranular space, which is formed at the Sch–CTB boundary. Attention is drawn to the fact that a very significant recrystallization of the crystals of the initial charge occurs. Along with small Sch crystals, relatively large (up to 150 μm) Sch crystals and its substitution products were found.

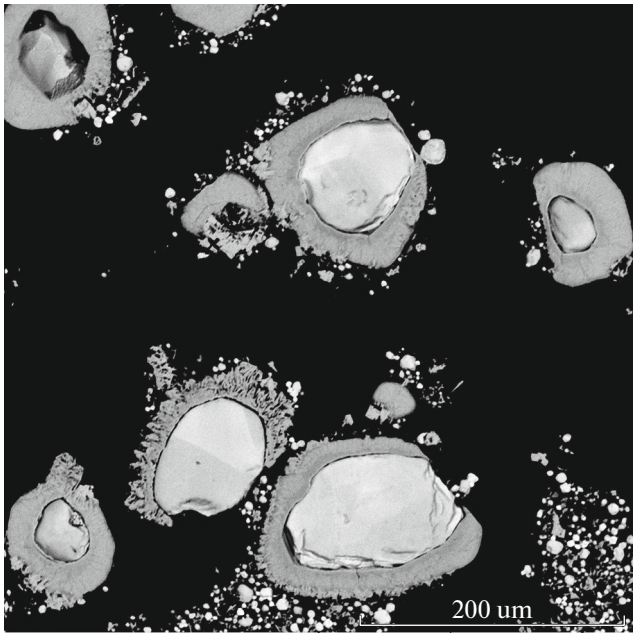

Fig. 2. Polished products of an experiment (no. 16) on the solubility of scheelite at 500°C and 100 MPa in Ni–NiO buffer in 0.316 *m* HCl solution.

X-ray patterns of the solid products of the experiments (Fig. 3) indicate that scheelite is in 0.01 *m* HCl remains almost pure; at 0.0316 *m* HCl, lines appear that are characteristic of WO_3; and, in solutions of 0.1 and 0.316 *m* HCl, there is a significant increase in reflections close to ⟨002⟩ (or ⟨001⟩), ⟨020⟩ , and ⟨200⟩ and a change in their intensities.

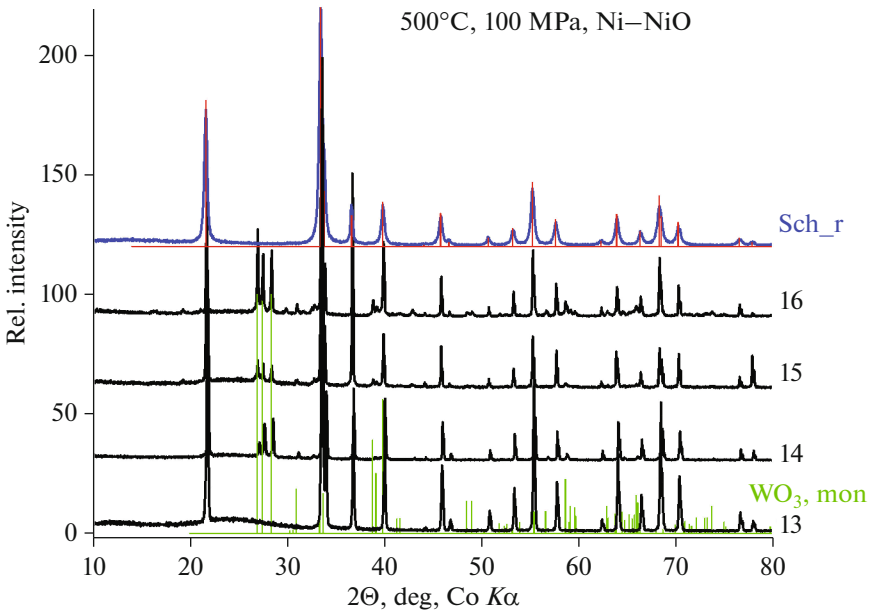

Fig. 3. Typical X-ray pattern of the experimental products (nos. 13–16). Legend: Sch_r, recrystallized scheelite (=PDF 85-0443), WO_3, monotungsten trioxide (PDF71-2141).

The Influence of Oxygen Buffers

In all experiments lasting 2 weeks, according to X-ray phase analysis, there were Co + CoO, Ni + NiO, Fe_3O_4 + Fe_2O_3, and Cu_2O + CuO buffer pairs, which indicates that a constant fugacity of oxygen (hydrogen) was maintained in the reactor and hydrogen-permeable platinum ampoules. In the products of experiments using cobalt–cobalt (II) oxide buffer, CoO accumulated, and the intensity of the Co lines decreased significantly compared to the initial mixture. In the nickel–bunsenite buffer, a slight increase in the intensity of the NiO lines was observed with a decrease in the characteristic lines of Ni. The cuprite–tenorite buffer initially contained almost pure CuO, and after experiments at 400 and 500°C partially recovered to Cu_2O. In experiments with iron-oxide buffer at 400°C, pure magnetite (Mgt) was used, which, according to the plan, should have been oxidized to hematite (Hem). However, no lines of hematite were found on the X-ray diffraction pattern of the solid products of the experiments. At the same time, a detailed analysis showed that, in addition to magnetite lines, the X-ray pattern contains maghemite γ-Fe_2O_3 (Mgh) lines and, thus, the equilibrium $f(O_2)$ was set with a magnetite–maghemite (Mgt–Mgh) buffer.

RESULTS AND DISCUSSION

Obviously, scheelite in HCl solutions in the studied concentration range from 0.01 to 0.316 mol/kg H_2O dissolved incongruently. In relatively dilute solutions containing from 0.01 to 0.0316 *m* HCl, in the experimental products, along with scheelite, insignificant amounts of WO_3 and/or WO_{3-x} tungsten oxides. The dissolution reaction of Sch with the formation of tungsten oxides can be represented as

$$CaWO_4 + 2H^+ = WO_{3-x} + Ca^{2+} + 0.5xO_2 + H_2O. \quad (1)$$

In solutions containing from 0.1 to 0.316 *m* HCl, formation of calcium tungsten–bronzes (CTBs) Ca_xWO_3 takes place, the average composition of which corresponds to the formula $Ca_{0.07}WO_3$. The formation of CTB proceeds according to the reaction

$$xCaWO_4 + (1-x)WO_3 = Ca_xWO_3 + 0.5xO_2. \quad (2)$$

WO_3 formed by reaction (1), when interacting with Sch, leads to the formation of CTB. The fact that in the experiments there is a consumption of WO_3, can be seen in the pictures of the samples. In the products of experiments carried out in solutions containing 0.316 *m* HCl, tungsten oxides are practically absent.

The results of the analysis of solutions allow us to estimate the amount of WO_3 formed during the dissolution of scheelite according to reaction (1). Since the weight of the reagents was carried controlled using the law of mass action at all stages of the experiments, it is not difficult to calculate the yield of WO_3. Calculations showed that a solution of 0.01 *m* HCl, interacting with Sch, leads to the formation of 1.6 ± 0.8 mol % WO_3 at 400 and 500°C. Redox conditions have little effect on the yield of WO_3 (or WO_{3-x}) in this solution. The sensitivity of the X-ray phase analysis method is not enough to identify WO_3; therefore, X-ray patterns show lines that are unique to Sch.

An increase in the concentration of HCl, as expected from the data in Table 1, promote the release of WO_3 (or WO_{3-x}). According to calculations, in a solution containing 0.0316 *m* HCl, the yield of the product is 4.8 ± 1.1 mol %, while it is 19.6 ± 6.0 in a solution of 0.1 *m* HCl and –58.1 ± 15.6 in a solution of 0.316 *m* HCl. Increasing the temperature reduces the output of WO_3, which is associated with an increase in the solubility of this phase.

According to (Cazzanelli et al., 1999), in the WO_3 phase, the following structural transitions take place: monoclinic or ε-phase from 5 to 278 K, triclinic or δ-phase from 278 to 290–300 K, monoclinic or γ-phase from 290–300 to 600 K, orthorhombic β-WO_3 from 600 to 1010 K, and tetragonal α-WO_3 from 1010 K to a melting point of 1746 K. When investigating industrial, chemically pure WO_3, Cherkashina et al. (Cherkashina et al., 2019) concluded that the triclinic phase is stable in the temperature range from 83 to 673 K, the X-ray diffraction pattern of which is very similar to the monoclinic WO_3 phase. Updated data on structural transitions are given in (Han et al., 2020). In the temperature range from 673 to 773 K that is of interest to us, according to (Salje, 1977; Woodward and Sleight, 1997; Voght et al., 1999; Han et al., 2020; Rao, 2013), there is an orthorhombic WO_3 related to the *Pmnb* (D_{2h}^{16}) structural group. The orthorhombic structure, according to the EPS spectra (Ghosh et al., 2017), has, in addition to W(VI), (35.8 eV ∈ $W4f_{7/2}$, 37.9 eV ∈ $W4f_{5/2}$ for W^{6+} particles), also a noticeable amount of W(V), as is indicated by the peaks at 34.5 and 37.2 eV related to $W4f_{7/2}$ $W4f_{5/2}$ fluctuations of W^{5+}. Research on $WO_{2.97}$ and $WO_{2.89}$ oxides (Mews et al., 2016) indicates the presence of W^{5+} only in the second phase, while, according to EPS spectra, there is predominantly W^{6+} in the $WO_{2.97}$ phase.

X-ray phase analysis does not allow us to accurately identify the structural type of stoichiometric newly formed WO_3 and WO_{3-x} oxides ($WO_{2.9}$ or $W_{20}O_{58}$, and $WO_{2.72}$ or $W_{18}O_{49}$), which are stable under the experimental parameters (Wriedt, 1989). The thermodynamically stable oxide phases in the W–O system are WO_3 (yellow), $WO_{2.9}$ (dark blue), and WO_2 (dark brown). Metastable $WO_{2.72}$ oxide of red-violet color was not found in the products of the experiments. Redox conditions, even with Co–CoO buffer, were not sufficient to reduce WO_3 and $WO_{2.9}$ to WO_2. The morphology of the tungsten oxides obtained in experiments is primarily associated with the physicochemical conditions of their formation (temperature, pressure, solution acidity, calcium concentration, oxygen fugacity). We do not rule out that, in WO_3 crystals formed at 673 and 773 K and 100 MPa in experiments lasting 14 days, upon cooling, structural transitions could occur: orthorhombic (β-WO_3 Pmnb) → monoclinic (γ-WO_3 P2,/n). It is also possible that the dehydration of W(VI) hydroxide formed at the initial stage of scheelite dissolution resulted in the precipitation of a metastable hexagonal oxide *h*-WO_3, which in the experiment mode turned into monoclinic γ-WO_3 (Lassner and Schubert, 1999). However, taking into account the relatively large size of the crystals and their color, we can conclude that, in experiments with 0.01 *m* HCl and Cu_2O–CuO buffer in equilibrium with the solution, it was monoclinic γ-WO_3. The crystals have the form of long, yellow needles (10–100 μm).

As for the dark-blue crystals of tungsten oxides (Lunk et al., 1993), which have the shape of parallelepipeds (close to rectangles), it is legitimate to classify these crystals as an orthorhombic allotropic modification $WO_{2.9}$ ($W_{20}O_{58}$) that is stable at 400 and 500°C. The parallelepiped shape of the crystals could be formed as a result of the dehydration of tungsten hydroxides (elpasalite), which is an intermediate product of the incongruent dissolution of scheelite (Lassner and Schubert, 1999).

Dark-blue formations on the surface of scheelite are the result of its successive replacement with a metastable hexagonal hydroxide or tungsten trioxide (*h*-WO_3) and subsequent transformation with recovery ($W^{6+} \rightarrow W^{5+}$) to hexagonal tungsten bronze (HTB) (Lassner and Schubert, 1999). The HTB structure has hexagonal and triangular channels along the *C* axis, through which metal cations and other particles with a positive charge can enter. According to (Lunk et al., 1993), the limiting composition of HTB, in which all channels are filled with A cations, corresponds to the formula $A_{0.33}WO_3$. Taking into account the data of analysis on an electron microscope, it can be argued that the composition of HTB can change from anhydrous cation-deficient $Ca_{0.07}WO_3$ to the ultimate saturated $(H_3O)_{0.19}Ca_{0.07}WO_3$.

Thus, the analysis of solid products showed that

• in solutions containing 0.01–0.0316 *m* HCl, at 400–500°C and 100 MPa, there are stable WO_3 tungsten oxides; and

• in solutions containing 0.1–0.316 *m* HCl, at 400–500°C and 100 MPa, there are stable hexagonal calcium–tungsten bronzes, in which the average molar ratio is Ca/W = 0.07.

The formation of WO_3 with incongruent dissolution of scheelite in acidic solutions was previously noted in the works (Rafalsky et al., 1984, 1974; Forster, 1977). According to (Forster, 1977), the solubility of scheelite in water at a pressure of 100 MPa depends on temperature and is in the range of 265–555°C is $(4–23) \times 10^{-6}$ mol/kg. In solutions of strong electrolytes (NaCl, KCl), the solubility of scheelite increases with an increase in the concentration of chlorides (ionic strength of the solution) and the acidity of the solution.

The introduction of calcium chloride into the test solution, on the contrary, reduces the solubility of

Sch. According to (Rafalsky et al., 1984), in 1 *m* NaCl solution in equilibrium with scheelite having pH = 3, adding 0.001 *m* $CaCl_2$ reduces *m* W from 5×10^{-5} to 3×10^{-6} mol/kg. The results of thermodynamic calculations of the solubility of scheelite in HCl solutions (pH range from 2 to 6) performed in the cited work yield values of *m* W that are 2–2.5 orders of magnitude lower than those presented in Table 1 for 400–500°C and 100 MPa for all the used oxygen buffers. Obviously, in the region of incongruent solubility, the tungsten content in the solution will be controlled by tungsten oxide or CTB, and the calcium content will be determined by the equilibrium of reaction (1). In the range of HCl concentrations from 0.1 to 0.316 mol/kg stable phases are scheelite and calcium–tungsten bronzes. Assuming that the composition of CTB corresponds to the formulas $Ca_{0.07}WO_3$ and/or $(H_3O)_{0.19}Ca_{0.07}WO_3$), then the data obtained are sufficient to refine the thermodynamic properties of CTB.

THERMODYNAMIC CALCULATIONS

As noted above, the data obtained indicate that scheelite at 400–500°C and 100 MPa in solutions of 0.01–0.316 *m* HCl dissolves incongruently. WO_3, $WO_{2.9}$, and calcium-containing HTB form during the experiments in dependance on *m* HCl and $f(O_2)$ during the experiments. These observations form the basis of thermodynamic calculations.

Obviously, when matching the thermodynamic properties of the components of an aqueous solution and solid phases that are in equilibrium with it, it is necessary to choose something as a basis. In our calculations, we used the following particles of an aqueous solution: H_2O, H^+, OH^-, Cl^-, HCl^0, Ca^{2+}, $CaCl^+$, $CaCl_2^0$, $CaOH^+$, $CaCl_2^0$, HWO_4^-, and HWO_4^- (Table 4) It is currently believed that the best thermodynamic data (equilibrium constants) for W(VI) particles are presented in (Wood and Samson, 2000). For W(V) particles, we (Redkin and Cygan, 2020) proposed $W_5O_{16}^{3-}$ (at 400°C) and WO_3^- and $H_2W_2O_7^-$ (at 500°C) species. For satisfactory agreement between the calculations and the experimental results, it is necessary to correct the thermodynamic properties (Gibbs free energies, entropy) of solid phases, which, as a rule, have a significant error, or to introduce new particles of an aqueous solution. In any case, it is necessary to analyze existing data and critically select them. The choice of a model for describing the activity coefficients of aqueous solution particles also affects the calculation results. It is known that increasing the temperature expands the limits of salt concentrations when using the Debye–Hückel equations, although there are numerous objections to this opinion.

The calculations were carried out using the Gibbs program (Shvarov, 2007). The individual particle-activity coefficients were calculated using the extended Debye–Hückel equation in the second approximation (Akinfiev et al., 2020). The dimensional parameter (effective ion radius) for all charged species is assumed to be 4.5 Å (Rafalsky, 1973; Rafalsky, 1973). The molal concentrations of Ca and W particles were used in the calculations. To do this, the result of modeling the content of elements in moles was divided by the mole fraction of water (water activity) in the solution.

When choosing the thermodynamic properties of solid phases (tungsten oxides, scheelite), a quantitative and qualitative analysis was carried out. As a result of the research, it was found that the existing thermodynamic data on redox equilibria in tungsten-oxide systems in the temperature range of 300–600°C have a significant inconsistency. Therefore, the values of free energies of WO_3(s) (Han et al., 2020) and WO_2(s) (Naumov et al., 1971), as well as G_T°, for $WO_{2.9}$ were calculated from the equilibrium constants of the reaction

$$20WO_3(s) = 20WO_{2.9}(s) + O_2(g),$$

from the data of (Chase_JANAF, 1998). $WO_{2.72}$ tungsten oxide was excluded from consideration due to the fact that, in the W–O system, it is stable at temperatures above 585°C at $P = 100$ Pa and above 640°C at 100 MPa. Quantities $\Delta H_{298.15}^\circ$ (and $\Delta G_{298.15}^\circ$) given by (Charlu and Kleppa, 1973; Chase_JANAF, 1998) have a significant (7 kJ/mol) negative deviation from the linear dependence of the composition for the extreme WO_2 and WO_3 phases.

The scheelite formation enthalpy was borrowed from the data of (Poling et al., 2008), while the entropy and the heat-capacity equation were taken from (Zhidikova and Khodakovskii, 1984). Calculations using data from (Wood and Samson, 2000) for Sch and (Chase_JANAF, 1998) for WO_3 and $WO_{2.9}$ lead to results that differ significantly from our experimental data at 400 and 500°C. The free energy of CTB was calculated from the results of experiments with Co–CoO buffer. It was noted that the $Ca_{0.07}WO_3$ and/or $(H_3O)_{0.19}Ca_{0.07}WO_3$ have equal values of ΔG_T° and the same solubility in HCl solutions, despite the fact that the apparent content of W(V) in them differs significantly—14 and 33 mol %, respectively. The values of the free energies of the formation of solid phases used in the calculations are presented in Table 5.

Since only W(VI) particles are involved in the calculations, $f(O_2)$ has little effect on the content of calcium and tungsten in a solution in equilibrium with scheelite. Figure 4 shows the results of thermodynamic modeling of the incongruent solubility of scheelite with the formation of WO_3, $WO_{2.9}$, and $Ca_{0.07}WO_3$ (or $(H_3O)_{0.19}Ca_{0.07}WO_3$) at 400 and 500°C and 100 MPa. Calculations showed that, under the conditions of a Cu_2O–CuO buffer ($f(O_2) = 3.98 \times 10^{-7}$ Pa) at 400°C, the region of congruent solubility of scheelite is at an HCl concentration below 4.34×10^{-3} *m*. At 500°C and fugacity of the Cu_2O–CuO buffer ($f(O_2) = 2.71 \times 10^{-4}$ Pa), the region of congruent solubility of scheelite is at an HCl concentration below 4.08×10^{-3} *m*. The solubility of

Table 4. Standard partial molar properties of particles at 298.15 K, 1 bar, and HKF parameters used in calculations

Particle	$\Delta_f G^\circ_{298}$ [a]	S°_{298} [b]	$a_1 \times 10$ [d]	$a_2 \times 10^{-2}$ [a]	a_3 [e]	$a_4 \times 10^{-4}$ [f]	c_1 [b]	$c_2 \times 10^{-4}$ [f]	$\omega \times 10^{-5}$ [a]	Link
H_2WO_4(aq)	−227742#	49.050#	8.1527	13.1578	1.2439	−3.7375	5.4299	−4.4806	−0.4028	# + Wood and Samson, 2000
HWO_4^-(aq)	−217130#	52.869#	−18.5862	7.1668	−0.7349	−2.4827	−15.4537	15.7442	0.0347	# + Wood and Samson, 2000
WO_4^{2-}(aq)	−216210#	2.128#	−3.8533	10.4708	4.4891	−3.2119	−10.0882	68.8178	4.0372	# + Wood and Samson, 2000
$CaCl_2$(aq)	−194000	6.000	6.2187	7.4058	2.8322	−3.0851	23.9610	3.2720	−0.0380	Sverjensky et al., 1997
$CaCl^+$	−163100	4.500	2.7148	−1.1497	6.1949	−2.7314	20.8839	0.5241	0.4862	Sverjensky et al., 1997
$CaOH^+$(aq)	−171490	−5.346	−2.2875	−13.3704	11.0053	−2.2263	14.5527	0.1431	−0.0820	Akinfiev and Zotov, 1999
Ca^{2+}	−132120	−13.500	−0.1947	−7.2520	5.2966	−2.4792	9.0000	−2.5220	1.2366	Johnson et al., 1992
HCl(aq)	−30410	3.200	1.2555	−4.7177	7.6043	−2.5840	16.7134	2.8727	−0.7000	Sverjensky et al., 1991
Cl^-	−31379	13.56	4.0320	4.8010	5.5630	−2.8470	−4.4000	−5.7140	1.4560	Johnson et al., 1992
O_2(aq)	3954	26.040	5.7889	6.3536	3.2528	−3.0417	35.3530	8.3726	−0.3943	Johnson et al., 1992
H_2(aq)	4236	13.800	5.1427	4.7758	3.8729	−2.9764	27.6251	5.0930	−0.2090	Johnson et al., 1992

Determined by the authors of the article. N. [a] cal/mol, [b] cal/mol/K, [c] cm^3/mol, [d] cal/mol/bar, [e] cal/K/mol/bar, [f] cal/K/mol, HKF particle parameters of HWO_4^-(aq) and H_2WO_4(aq) calculated from the values of K_p (Wood and Samson, 2000). * Thermodynamic properties of H_2O, H^+, and OH^- linked in the UNITHERM program and used automatically.

Sch in H_2O, according to calculations, is 2.78×10^{-6} and 2.93×10^{-6} mol/kg H_2O. An increase in the concentration of HCl leads to the precipitation of WO_3 from a solution. Complete replacement of Sch with the newly formed WO_3 phase takes place in solutions containing m HCl > 0.42 at 400°C and 0.56 at 500°C.

Under redox conditions corresponding to Fe_3O_4–Fe_2O_3 ($f(O_2) = 2.51 \times 10^{-19}$ Pa at 400°C), Ni–NiO ($f(O_2) = 3.78 \times 10^{-23}$ Pa at 400°C and 1.97×10^{-18} Pa at 500°C) and Co–CoO ($f(O_2) = 1.71 \times 10^{-24}$ Pa at 400°C and 8.16×10^{-20} Pa at 500°C) buffers, scheelite dissolves to form CTB. The region of congruent solubility of scheelite, as well as with Cu_2O–CuO buffer, has a rather narrow and limited m HCl < 2×10^{-3}. In solutions containing m HCl > 0.36, at a given scheelite ratio/solution = 0.18 mol Sch/1000 g H_2O and 400°C, the stable phase is WO_3. According to calculations, the impact of solutions containing m HCl > 0.56 per 0.22 mol Sch at 500°C and fO_2 (Ni–NiO) leads to the formation of WO_3, while $WO_{2.9}$ oxide is produced in the case of Co–CoO buffer.

Figure 5 shows the results of modeling the Sch solubility in solutions of 0.001–1.0 m KCl on the lines of hydrolysis equilibrium of microcline (Mic) with quartz (Qtz) and muscovite (Ms),

$$1.5\text{Mic} + \text{HCl} = 3\text{Qtz} + 0.5\text{Ms} + \text{KCl},$$

at 400 and 500°C and P = 100 MPa. The calculations were used thermodynamic data from (Redkin and Cygan, 2020) that were consistent with experiments (Hemley, 1959; Redkin, 1983). According to calculations, the dissolution of Sch at 400 and 500°C occurs congruently in KCl solutions and oxygen fugacity (Co/CoO, Ni/NiO, and Cu_2O/CuO buffers) does not affect the calculation results. There is a satisfactory agreement with the experimental data of Foster (Foster, 1977) at 400 and 500°C and P = 100 MPa. According to calculations, the main contribution to the scheelite solubility is made by the HWO_4^- particle. An increase in the solubility of scheelite is associated mainly with an increase in the ionic strength of the solution (Bryzgalin, 1976).

Table 5. Free energies of formation of tungsten-containing solid phases at P = 100 MPa used in these calculations

T, °C	g°_T, kJ/mol			
	$CaWO_4$	$Ca_{0.07}WO_3$	WO_3	$WO_{2.9}$
400	−1592.600	−849.257	−802.178	–
500	−1599.000	−859.671	−820.620	−798.310

Taking into account that the concentration of sodium salts in natural hydrothermal solutions is higher than that of potassium salts, we performed calculations based on the solubility of scheelite in NaCl–KCl–HCl solutions. Because the composition of ore-bearing solutions is not known to us, but it is known that they produce quartz–muscovite alteration of host rocks, then boundary conditions can be introduced. The Qtz + Ms association field, according to (Meier and Hemley, 1967) at 500 and 400°C, 100 MPa, and m Cl = const is limited to the following invariant points: Qtz–Ab (albite)–Mic–Ms, Qtz–Ab–Prg (paragonite)–Ms, and Qtz–And (andalusite)–Prg–Ms (at 500°C) or Qtz–Pf (pyrophyllite)–Prg–Ms (at 400°C). The thermodynamic data for all Al–Si phases used in (Redkin and Cygan, 2020) are presented in Table 6. Obviously, if the concentration of chlorides in the system changes, then the invariant points turn into hydrolysis equilibria, which determine the m KCl/m HCl and m NaCl/m HCl ratios. Thus, the solubility of Sch on the reaction lines of the hydrolysis of aluminosilicates will correspond to the limiting values.

Figure 6 shows the results of calculating the Sch solubility in (Na, K)Cl solutions in a system in which

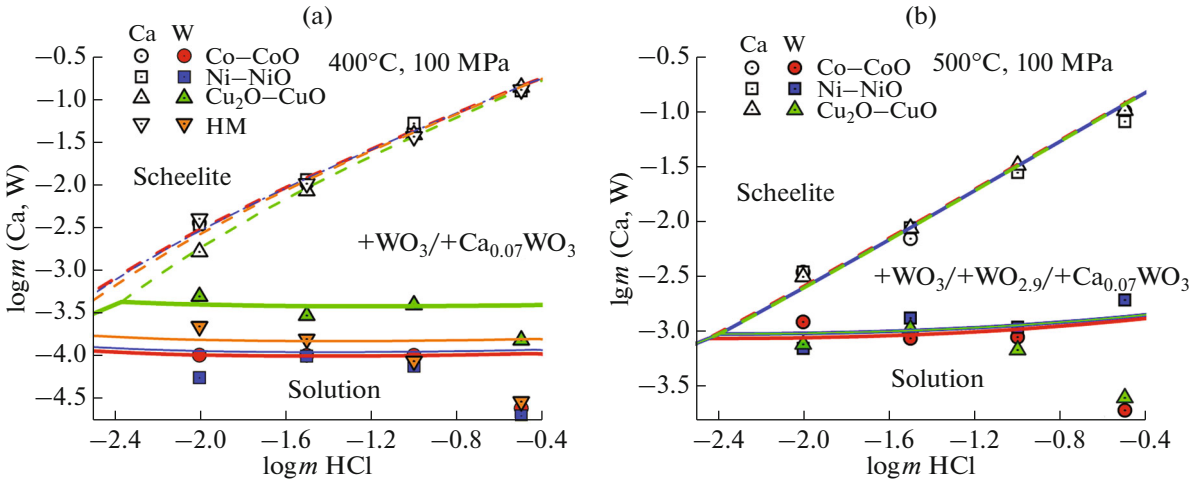

Fig. 4. Influence of m HCl on content of m W and Ca in solution in equilibrium with scheelite at 400 and 500°C, P = 100 MPa and oxygen fugacity given by various metal oxide buffers, according to experimental (symbols) and calculated (lines) data.

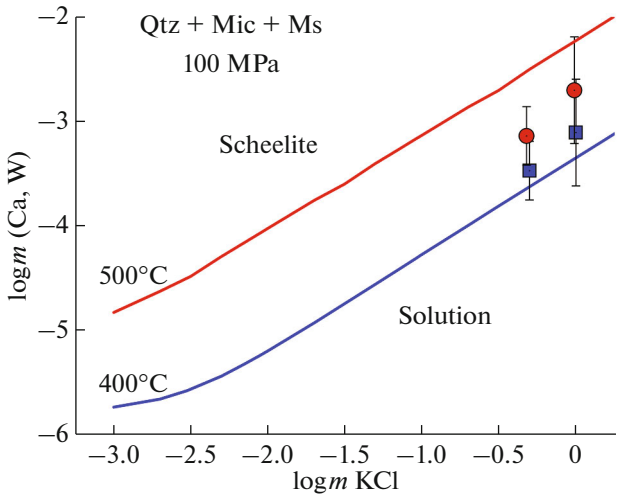

Fig. 5. Influence of *m* KCl on content of *m* W and Ca in a solution in equilibrium with scheelite under conditions controlled by a quartz–microcline–muscovite buffer at 400 and 500°C and 100 MPa and oxygen fugacity given by nickel–bunsenite buffer according to experimental data ((Foster, 1977), symbols: square, 400°C; round, 500°C) and calculated (lines) data.

the acidity of solutions and redox conditions are controlled by aluminosilicate buffers and metal-oxide buffers. The calculations were performed at 400 and 500°C, pressure 100 MPa. Scheelite has been shown to dissolve congruently in solutions controlled by buffers Qtz–Ab–Mic–Ms, Qtz–Ab–Prg–Ms, and Qtz–And–Prg–Ms at 500°C and Qtz–Ab–Mic–Ms and Qtz–Ab–Prg–Ms at 400°C. The redox conditions do not affect the concentration of tungsten in solution due to the fact that under the conditions under consideration (500°C, 100 MPa, *m* KCl, fO_2) the only solid phase containing W(VI) is stable: Sch. The tungsten content increases with the total chloride concentration and with the acidity of the Al–Si buffer (Fig. 6).

According to calculations, under the conditions of the Qtz–Pf–Prg–Ms buffer at 400°C and 100 MPa in solutions containing $m\ Cl_{init} = m\ (NaCl + KCl)_{init} > 0.094$, along with Sch, tungsten trioxide—WO_3—is stable. Hydrothermal tungsten deposits are not characterized by the simultaneous presence of Sch and WO_3. Gas–liquid inclusions in minerals at tungsten deposits testify to the high salinity of high-temperature hydrothermal solutions (Wood and Vlassopoulos, 1989). Obviously, the ore-bearing solutions did not exist by themselves, but were in a state close to equilibrium with the host aluminosilicate rocks, the role of which is similar to the considered buffers. Because solutions in which WO_3 is formed should be excluded from consideratio$_n$, then it follows that the acidity ($m\ H^+$) of tungsten–ore solutions was lower than given by the Qtz–Pf–Prg–Ms buffer at 400°C to 0.1 *m* (Na,K)Cl solution. The equilibrium ratio can be considered as an indicator of the acidity of the Al-Si buffer association $m\ Na^+/m\ H^+$ (or $m\ K^+/m\ H^+$). If we assume that the main mechanism of scheelite precipitation from solution was the cooling of the latter, it can be shown that solutions are saturated with scheelite and in equilibrium with Qtz–Ab–Mic–Ms and Qtz–Ab–Prg–Ms mineral associations at 500°C and 100 MPa when the temperature changes up to 400°C are capable of depositing 90–92% of Sch.

Comparison of solubility data for ferberite (Redkin and Cygan, 2020) and scheelite (Fig. 6) in Al–Si buffer systems can be used to assess the equilibrium of these ore phases in the chloride system. According to thermodynamic calculations, the value of $m\ Ca_{aq}/(m\ Ca_{aq} + m\ Fe_{aq})$ depends on the ionic strength of the solution and is 0.41 ± 0.03 and 0.78 ± 0.08 at 500 and 400°C and 100 MPa for Qtz–Ab–Mic–Ms and Qtz–Ab–Prg–Ms. These values are in good agreement with the experimental data (Korzhinskaya and Zaraisky, 1997) according to the exchange equilibrium $Ferb + CaCl_2 = Sch + FeCl_2$ studied under conditions of Ni–NiO buffer.

CONCLUSIONS

The solubility of scheelite in HCl solutions at 400 and 500°C, $P_{total} = 100$ MPa. It was found that Sch in HCl solutions from 0.01 to 0.316 *m* dissolves incongruently to form WO_3, $WO_{2.9}$, and calcium–tungsten bronzes, the average composition of which corre-

Table 6. Standard thermodynamic properties of Al–Si solid phases adopted in the present calculations

Mineral	$\Delta_f G^\circ_{298}$	S°_{298}	V_{298}	$C^\circ_p = a + bT \times 10^{-3} + cT^{-2} \times 10^5 + dT^{-0.5} + fT^2$			Source
index	J/mol	J/(mol K)	J/bar	*a*	*b*	*c*	
Ab	−3715775#	194.20#	10.007	583.94	−92.852	16.78*	Robie et al., 1978
And	−2417980#	93.220	4.9900#	164.42#	33.594#	−46.078#	Robie et al., 1978
Mic	−3742330	214.2	10.872	759.55	−217.11	47.642*	Robie et al., 1978
Ms	−5600547#	245.000#	14.0810	917.70	−81.11	28.34*	Robie et al., 1995
Pf	−5240840#	239.400#	12.8100	−87.4007	847.683	−45.1557*	Krupka et al., 1979
Prg	−5546450#	277.82	13.253	407.647	102.508	−110.625	Pokrovsky, 1984
Qtz	−856240	41.340	2.2688	46.940	34.31	−11.30	Helgeson et al., 1978

The authors; * Ab: $d = -6.4242 \times 10^3$, $f = 2.2722 \times 10^{-5}$; Mic: $d = -9.5268 \times 10^3$, $f = 6.4333 \times 10^{-5}$; Ms: $d = -1.0348 \times 10^4$; Pf: $d = 4.31112 \times 10^3$, $f = -4.51557 \times 10^{-4}$.

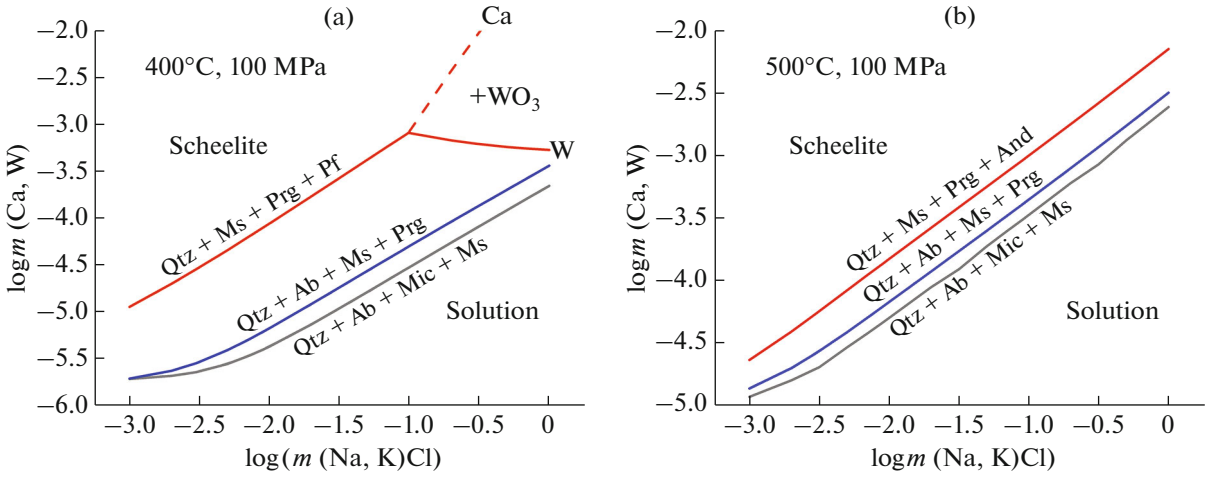

Fig. 6. Influence of chloride concentration (NaCl, KCl) on scheelite solubility at (a) 400 and (b) 500°C and 100 MPa with Cu_2O–CuO buffers and acidity regulated by Al–Si associations Qtz + Ab + Mic + Ms, Qtz + Ab + Ms + Prg, and Qtz + Pf + Ms + Prg (at 400°C) and Qtz + And + Ms + Prg (at 500°C). With $+WO_3$, scheelite dissolves incongruently with the formation of tungsten trioxide.

sponds to the formula $Ca_{0.07}WO_3$. An increase in HCl concentration promotes the release of WO_3 (or WO_{3-x}). Increasing the temperature reduces the output of WO_3, which is associated with an increase in the solubility of this phase.

Based on the analysis of the obtained experimental data, the free energies of formation of WO_3 and $WO_{2.9}$ tungsten oxides, as well as scheelite and calcium–tungsten bronze, were determined. Using mutually consistent thermodynamic data, the solubility of Sch in HCl and (Na,K)Cl solutions with the participation of aluminosilicate buffers was calculated. It is shown that scheelite has a wide range of congruent solubility in salt systems.

ACKNOWLEDGMENTS

The authors are grateful to A.N. Nekrasov (Korzhinskii Institute of Experimental Mineralogy, Russian Academy of Sciences) for assistance in microprobe analyses, N.A. Drozhzhina (Korzhinskii Institute of Experimental Mineralogy, Russian Academy of Sciences) for X-ray analysis of the solid products of the experiments, and V.K. Karandashev (Institute of Microelectronics Technology and High-Purity Materials, Russian Academy of Sciences) for ICP analysis of the solutions after the experiments. We are grateful to the reviewer N.N. Akinfiev, Dr. Sci., for valuable remarks and useful recommendations.

FUNDING

Thos work was supported by the Russian Foundation for Basic Research (grant no. 20-05-00307a) and Program of Fundamental Research of the State Academies of Sciences FMUF-2022-0003.

CONFLICT OF INTEREST

The authors declare that they have no conflicts of interest.

OPEN ACCESS

REFERENCES

Akinfiev, N. and Zotov, A., Thermodynamic description of equilibria in mixed fluids (H_2O–non-polar gas) over a wide range of temperature (25–700°C) and pressure (1–5000 bars), *Geochim. Cosmochim Acta,* 1999, vol. 63, nos. 13–14, pp. 2025–2041.

Akinfiev, N.N., Korzhinskaya, V.S., Kotova, N.P., Redkin, A.F., and Zotov, A.V., Niobium and tantalum in hydrothermal fluids: thermodynamic description of hydroxide and hydroxofluoride complexes, *Geochim. Cosmochim Acta,* 2020, vol. 280, pp. 102–115.

Bryzgalin, O.V., On solubility of wolframic acid in aqueous–salt solutions at high temperatures, *Geokhimiya,* 1976, no. 6, pp. 864–870.

Cazzanelli, E., Vinegoni, C., Mariotto, G., Kuzmin, A., and Purans, J., Low-temperature polymorphism in tungsten trioxide powders and its dependence on mechanical treatments, *J. Solid State Chem.,* 1999, vol. 143, pp. 24–32.

Charlu, T.V. and Kleppa, O.J., High-temperature combustion calorimetry 1. Enthalpies of formation of tungsten oxides, *J. Chem. Thermodynam.,* 1973, vol. 5, pp. 325–330.

Chase, Jr.M.W., *NIST-JANAF Thermochemical Tables, J. Phys. Chem. Ref. Data, Monogr.,* no. 9, New York: American Institute of Physics for the National Institute of Standards and Technology, 1998.

Cherkashina, N.I., Pavlenko, V.I., and Yastrebinskii, R.N., Phase transitions and change of electrophysical properties of WO_3 in the temperature range of 83–673 K, *Izv. Vussh. Ucheb. Zaved., Fizika,* 2019, vol. 62, no. 5 (737), pp. 126–131.

Foster, R.P., Solubility of scheelite in hydrothermal chloride solutions, *Chem. Geol.,* 1977, vol. 20, no. 1, pp. 7–43.

Ghosh, K., Roy, A., Tripathi, S., Ghule, S., Singh, A.K., and Ravishankar, N., Insights into nucleation, growth and phase selection of WO_3: morphology control and electrochromic properties, *J. Mater. Chem.,* 2017, vol. 5, pp. 7307–7316.

Han, B., Khoroshilov, A.V., Tyurin, A.V., Baranchikov, A.E., Razumov, M.I., Ivanova, O.S., Gavrichev, K.S., and Ivanov, V.K., WO_3 thermodynamic properties at 80–1256 K revisited, *J. Therm. Anal. Calorimetry,* 2020, vol. 142, pp. 1533–1543.

Helgeson, H.C., Delany, J.M., Nesbitt, H.W., and Bird, D.K., Summary and critique of the thermodynamic properties of rock-forming minerals, *Am. J. Sci.,* 1978, vol. 278.

Hemley, J.J., Some mineralogical equilibria in the system K_2O–Al_2O_3–SiO_2–H_2O, *Am. J. Sci.,* 1959, vol. 257, pp. 241–270.

Hu, W., Tong, W., Li, L., Zheng, J., and Li, G., Cation non-stoichiometry in multi-component oxide nanoparticles by solution chemistry: a case study on $CaWO_4$ for tailored structural properties, *Phys. Chem.,* 2011, vol. 13, pp. 11634–11643.

Johnson, J.W., Oelkers, E.H., and Helgeson, H.C., Supcrt92: a software package for calculating the standard molal thermodynamic properties of minerals, gases, aqueous species, and reactions from 1 to 5000 bar and 0 to 1000°C, *Comp. Geosci.,* 1992, vol. 18, no. 7, pp. 899–947.

Khodokovskiy, I.L. and Mishin, I.V., Solubility products of calcium molybdate and calcium tungstate; ratio of powellite to scheelite mineralization under hydrothermal conditions, *Int. Geol. Rev.,* 1971, vol. 13, no. 5, pp. 760–768.

Korzhinskaya, V.S. and Zaraiskii, G.P., Experimental study of the scheelite–ferberite equilibrium in chloride fluid at T = 300–600°C and P = 1 kbar, *Dokl. Earth Sci.,* 1997, vol. 353A, no. 3, pp 457–460.

Krupka, K.M., Robie, R.A., and Hemingway, B.S., High-temperature heat capacities of corundum, periclase, anorthite, $CaAl_2Si_2O_8$ glass, muscovite, pyrophyllite, $KAlSi_3O_8$ glass, grossular, and $NaAlSi_3O_8$ glass, *Am. Mineral.,* 1979, vol. 64, nos. 1–2, pp. 86–101.

Lassner, E. and Schubert, W.-D., *Tungsten: Properties, Chemistry, Technology of the Element, Alloys, and Chemical Compounds,* New York: Kluwer Academic Press, 1999.

Lunk, H.-J., Ziemer, B., Salmen, M., and Heidemann, D., What is behind 'tungsten blue oxides?, *Proceedings of the 13 International Plansee Seminar,* Bildstein H. and Eck, R., Eds., Reutte: Metallwerk Plansee, 1993, vol. 1, pp. 38–56.

Mews, M., Korte, L., and Rech, B., Oxygen vacancies in tungsten oxide and their influence on tungsten oxide/silicon heterojunction solar cells, *Sol. Ener. Mater. Sol. Cells,* 2016, vol. 158, pp. 77–83.

Meyer, C. and Hemley, J.J., Wall rock alteration, *Geochemistry of Hydrothermal Ore Deposits,* 1st Edition, Barnes, H., Ed., New York: Holt Rinehart & Winston, 1967, pp. 166–235.

Naumov, G.B., Ryzhenko, B.N., and Khodakovskiy, I.L., *Spravochnik termodinamicheskikh velichin (dlya geologov)* (A Handbook of Thermodynamic Data: For Geologists), Moscow: Atomizdat, 1971.

Pokrovskii, V.A., Study of Mineral Reactions in Model Hydrothermal Systems, *Extended Abstract of Candidate's (Geol.-Min.) Dissertation,* Moscow: MGU, 1984.

Poling, B.E., Thomson, G.H., Friend, D.G., Rowley, R.L., and Wilding, W., *Section 2. Physical and Chemical Data, Perry's Chemical Engineers' Handbook, 8-th Edition,* Green, D.W. and Robert, P.E. Eds., New York: McGraw-Hill Companies, 2008. Doi: https://doi.org/10.1036/0071511245

Rafal'skii, R.P., *Gidrotermal'nye ravnovesiya i protsessy mineraloobrazovaniya* (Hydrothermal Equilibria and Processes of Mineral Foramtion), Moscow: Atomizdat, 1973.

Rafal'skii, R.P., Bryzgalin, O.V., and Fedorov, P.L., A transfer of tungsten and precipitation of scheelite under hydrothermal conditions, *Geokhimiya*, 1984, no. 5, pp. 611–624.

Rao, M.C., Structure and properties of WO_3 thin films for electrochromic device application, *J. Non-Oxide Glasses,* 2013, vol. 5, no. 1, pp. 1–8.

Red'kin, A.F., Experimental and Thermodynamic Study of Reactions Controlling Conditions of Formation of Wall-Rock Beresites, *Extended Abstract of Candidate's (Geol.-Min.) Dissertation,* Moscow GEOKhI AN SSSR, 1983.

Redkin, A.F. and Cygan, G.L., Experimental determination of ferberite solubility in the KCl–HCl–H_2O system at 400–500°C, and 20–100 MPa, In *Advances in Experimental and Genetic Mineralogy*, Litvin, Yu. and Safonov, O., Eds., New York: Springer, 2020.

Robie, R.A., Hemingway, B.S., and Fisher, J.R., Thermodynamic properties of minerals and related substances at 298.15 K and 1 bar (105 pascals) pressure and at higher temperatures, *U.S. Geol. Surv. Bull.,* 1978, No. 1452.

Robie, R.A. and Hemingway, B.S., Thermodynamic properties of minerals and related substances at 298.15 K and 1 bar (105 pascals) pressure and at higher temperatures, *U.S. Geol. Surv. Bull.,* 1995, no. 2131.

Salje, E., The orthorhombic phase of WO_3, *Acta Crystallogr.,* 1977, pp. 574–577.

Shvarov, Yu.V., On thermodynamic models for real solutions, *Geochem. Int.,* 2007, vol. 45, no. 6, pp. 606–614.

Sverjensky, D.A., Hemley, J.J., and D'Angelo, W.M., Thermodynamic assessment of hydrothermal alkali feldspar–mica–aluminosilicate equilibria, *Geochim. Cosmochim. Acta,* 1991, vol. 55, pp. 989–1004.

Vogt, T., Woodward, P.M., and Hunter, B.A., The high-temperature phases of WO_3, *J. Solid State Chem.,* 1999, vol. 144, pp. 209–215.

Wood, S.A. and Samson, I.M., The hydrothermal geochemistry of tungsten in granitoid environments: I. Relative solubilities of ferberite and scheelite as a function of T, P, pH, and mNaCl, *Econ. Geol. Bull. Soc. Econ. Geol.,* 2000, vol. 95, no. 1, pp. 143–182.

Wood, S.A. and Vlassopoulos, D., Experimental determination of the hydrothermal solubility and speciation of tungsten at 500°C and 1 kbar, *Geochim. Cosmochim. Acta,* 1989, vol. 53, pp. 303–312.

Wriedt, H.A., The O–W (oxygen–tungsten) system, *Bull. Alloy Phase Diagrams,* 1989, vol. 10, no. 4, pp. 368–384.

Zhidikova, A.P. and Khodakovskii, I.L., *Termodinamicheskie svoistva ferberita, gyubnerita, sheelita i povelita. Fiziko-khimicheskie modeli petrogeneza i rudoobrazovaniya* (Thermodynamic Properties of Ferberite, Gubnerite, Scheelite, and Powellite. Physicochemical Models of Petrogenesis and Ore Formation), Novosibirsk: Nauka, 1984.